Article

Spectroscopic and Structural Properties of β-Tricalcium Phosphates Ca$_9$RE(PO$_4$)$_7$ (RE = Nd, Gd, Dy)

Veronica Paterlini [1,2,*], **Asmaa El Khouri** [3], **Marco Bettinelli** [1], **Daniele Maria Trucchi** [4] **and Francesco Capitelli** [5,*]

1 Luminescent Materials Laboratory, Verona University, Ca' Vignal, Strada Le Grazie 15, 37134 Verona, Italy; marco.bettinelli@univr.it
2 Department of Materials and Environmental Chemistry, Stockholm University, 106 91 Stockholm, Sweden
3 Semlalia Faculty of Sciences, BP 2390, Cadi Ayyad University, Marrakech 40000, Morocco; elkhouriasma@gmail.com
4 Institute of Structure of Matter—CNR, Via Salaria Km 29.300, 00016 Monterotondo (Rome), Italy; daniele.trucchi@ism.cnr.it
5 Institute of Crystallography—CNR, Via Salaria Km 29.300, 00016 Monterotondo (Rome), Italy
* Correspondence: veronica.paterlini@mmk.su.se (V.P.); francesco.capitelli@ic.cnr.it (F.C.); Tel.: +39-340-315-1930 (V.P.); +39-069-067-2616 (F.C.)

Abstract: Rare-earth-based Ca$_9$RE(PO$_4$)$_7$ (RE = Nd, Gd, Dy) materials were synthesized by solid-state reaction at T = 1200 °C. The obtained tricalcium phosphate (TCP) materials are efficient light emitters due to the presence of RE^{3+} ions, although these ions are present at high concentrations. Moreover, in these host structures, these ions can be used as optical probes to study their local environments. Thus, photoluminescence (PL) emission spectra of the powder samples clearly indicated, for Dy^{3+} and Gd^{3+} ions, the presence of the RE^{3+} ion in low-symmetry sites with some local structural disorder, and the spectra show the presence of vibrational features (in the case of Gd^{3+}). For the Nd^{3+} phase, emission bands are present around 900, 1050, and 1330 nm, originating from the ^{4}F$_{3/2}$ level. In general, these RE-TCP samples are interesting luminescent materials in the visible (Dy), UV (Gd), and NIR (Nd) regions, due to weak concentration quenching even for high concentrations of the emitting ion.

Keywords: TCP; rare-earth elements; luminescence spectroscopy; structural investigation

1. Introduction

Tricalcium phosphate (TCP)-based materials, such as Ca$_3$(PO$_4$)$_2$ and Ca$_9$RE(PO$_4$)$_7$ (RE = rare earth), are interesting as hosts for luminescent ions. They are isotypic with a whitlockite structure, and thus they are characterized by the presence of five different crystal sites having different coordination numbers and by intrinsic structural disorder [1–3]. These sites are suitable for substitution with several dopant ions [3–5]. The effects on the crystal structure after substitution of the Ca^{2+} sites with different RE^{3+} ions has been studied in relation to the doping amount and the ionic radius of the dopant [2,5]. The luminescence properties were found to be dependent on the site distribution and crystal structure [2]. Most of the studied materials involve the introduction of the emitting ion as an impurity. Structural and optical properties of RE^{3+}-doped calcium-phosphate-based materials have been investigated in several hosts and with different RE^{3+} ions as dopants as well as bulk constituents [1–7]. The presence of multiple sites and their peculiar distribution in whitlockite-type structures have been shown to be suitable for obtaining light emission even in the presence of concentrated materials [3], mainly thanks to their inefficient concentration quenching [3,8,9].

Some of these compounds doped with RE^{3+} ions have also shown applications as lighting emitting materials, scintillating materials [1,4], in vivo imaging [2,10], and thermoluminescent dosimeters (TLD) [11]. The study of absorption and emission characteristics

of a phosphor enables the understanding of electronic energy levels in the host crystal and, consequently, the development of new phosphors of practical relevance [12].

Concentrated materials based on Eu^{3+} and Tb^{3+} have been employed, thanks to their efficient emission in the red and green, respectively, often with a high Tb^{3+} concentration doped with Eu^{3+} to obtain an energy transfer mechanism (ET) [3]. Moreover, due to the role of Eu^{3+} as a structural probe, its luminescence has allowed the study of local symmetry in these materials [13].

In order to further expand the study of $Ca_9RE(PO_4)_7$ materials, Dy^{3+}, Gd^{3+}, and Nd^{3+} ions were employed as bulk constituents and their luminescence properties were investigated in relation to their structure. Up to now, the luminescence of these specific ions has been investigated in TCP hosts only at low doping concentrations (lower that 10%) or in combination with other RE^{3+} ions for several applications [14], but not as bulk constituents. Moreover, the lifetime analysis has generally been omitted [11,15].

In this work, the relative intensity of Dy^{3+} emission bands, as well as its decay kinetics, were investigated to give more insight into the local disorder of the host, showing the possible presence of multiple emitting centers that are mutually interacting through non-radiative mechanisms.

However, the characteristic transitions of Gd^{3+} are strongly related to the surrounding host vibrations and are dependent on the nature of the lattice. Comparison of the emission bands with the vibrational modes occurring in the FTIR spectrum also made this ion a good optical probe with which to investigate the structural features of the host materials [9,16,17].

The aim of the present work was to provide a study of the optical spectroscopy of $Ca_9RE(PO_4)_7$ (RE = Nd, Gd, Dy) TCP materials obtained from a solid state reaction and to relate the luminescence features to the structures of the materials.

2. Experimental

Synthesis. $Ca_9RE(PO_4)_7$ (RE = Nd, Gd, Dy) β–TCP were synthesized by solid state reaction from a mixture of reagent-grade $CaCO_3$, $CaHPO_4$, and pertinent rare-earth oxides RE_2O_3 (RE = Nd, Gd, Dy), according to the method of Lecointre et al., 2010 [18]:

$$4 \cdot CaCO_3 + 14 \cdot CaHPO_4 + RE_2O_3 \rightarrow 2 \cdot Ca_9RE(PO_4)_7 + 7 \cdot H_2O + 4 \cdot CO_2$$
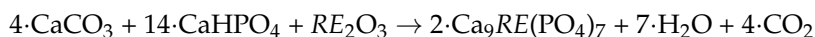
After a first heating cycle at 400 °C for 6 h, performed in order to remove H_2O and CO_2 from the mixture, the different powder samples were ground in an agate mortar and calcined again in an alumina crucible for 12 h at 1200 °C [6].

X-ray diffraction (XRD). The powder XRD data of the title compounds for qualitative and structural analysis were recorded at room temperature on a Bruker D8 diffractometer using Cu Kα radiation ($\lambda_{K\alpha}$ = 1.54056 Å) and equipped with a lYNXEYE detector. The measures were achieved in Bragg–Brentano geometry (angular range = 10–70° (2θ); step size of 0.06° (2θ); data collection time = 18 min). Main acquisition parameters are reported in [6].

Fourier Transform Infrared (FTIR) spectroscopy. Powder spectra of the title compounds were collected on a Nicolet iS50 FTIR spectrometer equipped with a DTGS detector and a KBr beamsplitter; the nominal resolution was 4 cm^{-1}; 64 scans were averaged for both sample and background. The samples were prepared as KBr disks, mixing ca. 1 mg of RE-TCP powder with 150 mg of potassium bromide. Experimental details are reported in [6].

Photoluminescence spectroscopy. Room temperature luminescence spectra were achieved by using a Fluorolog 3 (Horiba-Jobin Yvon) spectrofluorometer, equipped with a continuous Xe lamp as the excitation source for steady state measurements, a double excitation monochromator, and a single-emission monochromator (mod. HR320). A photomultiplier in photon counting mode was employed for the detection of the emitted signal up to 800 nm, while a CCD array detector Symphony II cooled by liquid nitrogen was used to measure in the NIR region.

Lifetimes were collected with the same instrument, with a xenon microsecond pulsed lamp as the excitation source. The decay curves were measured by means of a time-correlated single-photon counting technique (TCSPC) and were fitted by the instrument software [19].

3. Discussion

3.1. β–TCP Structural Arrangment

3.1.1. β-TCP and Related Phases

B-tricalcium phosphate, $Ca_3(PO_4)_2$ (β-TCP), is a high-temperature phase usually obtained by thermal decomposition at T = 800 °C of Ca-deficient HAp, or by solid-state reaction of acidic Ca orthophosphate with a base, usually CaO. β-TCP is rhombohedral with space group $R3c$ ($a = b = 10.4352(2)$ Å; $c = 37.4029(5)$ Å; $V = 3527.26$ Å^3 [20]) and, at T > 1125 °C, changes into the polymorph phase α–TCP, monoclinic in $P2_1/a$ ($a = 12.887(2)$ Å; $b = 27.280(4)$; $c = 15.219(2)$ Å; $β = 126.20(1)°$; $V = 4317.52$ Å^3 [21]); the β → α transition in TCP may occur later at a higher temperature in the presence of RE_2O_3 reactants [6], as in the case of the present *RE*-TCP samples calcined at 1200° (see Synthesis paragraph) but displaying a β–TCP structure as described later. β-TCP has its natural counterpart in the isotypic mineral whitlockite, ideally $Ca_9Mg(PO_4)_6[PO_3(OH)]$, rhombohedral in $R3c$ ($a = b = 10.357(3)$ Å, $c = 37.095(15)$ Å and $V = 3446(2)$ Å^3) [22]; because of isotypicity among natural whitlockite and β-TCP, the latter is often indicated as synthetic whitlockite, and its structure is indicated as whitlockite-type. TCP presents a third polymorph, the high-pressure form known as γ-TCP, rhombohedral in $R-3m$, usually coming from transformation both at high temperature and pressure of β-TCP [23]; it is also found with mineral name *tuite* in chondritic meteorites, as a result of shock impact of other calcium phosphate minerals [24]. Last, the occurrence of a trivalent cation (RE^{3+}, but also Fe^{3+}, Cr^{3+}) in the β-TCP structure leads to the present formula $Ca_9RE^{3+}(PO_4)_7$ [6].

3.1.2. XRD Qualitative Analysis

Qualitative analysis of the powder XRD profiles of the $Ca_9RE(PO_4)_7$ (*RE* = Nd, Gd, Dy) underlined the matching between the experimental profiles and undoped *β*-TCP, highlighting the single-phase behavior for all the three powder samples [6]. XRD spectra were deposited at the PDF-2 database [25] with card numbers 00-070-0125 (Nd), 00-070-0127 (Gd), and 00-070-0128 (Dy). Powder XRD patterns are reported in Figure 1a (Nd), Figure 1b (Gd), and Figure 1c (Dy).
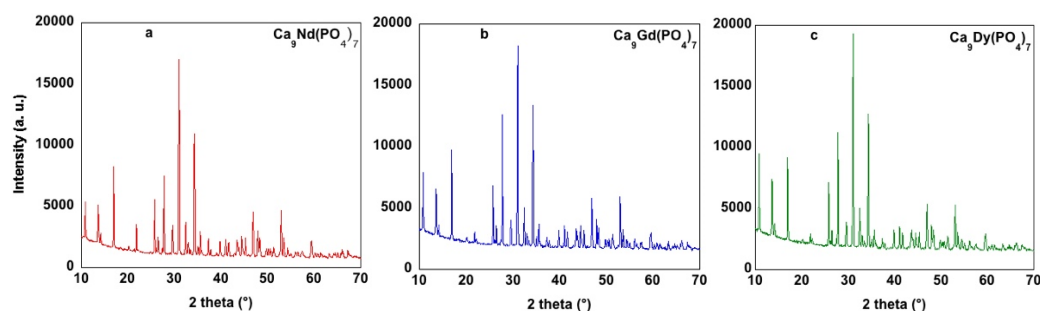

Figure 1. Powder X-ray spectra of $Ca_9Nd(PO_4)_7$ (**a**), $Ca_9Gd(PO_4)_7$ (**b**), and $Ca_9Dy(PO_4)_7$ (**c**).

3.1.3. Polyhedral Environment

As a preliminary remark, structural features of $Ca_9RE^{3+}(PO_4)_7$ compounds are strongly dependent on the *lanthanide contraction* effect [26], a physical property of those particular rare-earth elements called 'lanthanides' (*Ln*), from La (Z = 57) up to Lu (Z = 71), i.e., the decrease in ionic radius. This causes in *RE*-bearing compounds a certain similarity in crystal-chemical features, such as lattice parameters and cell volume, which usually slightly decrease going across the *RE* series (from La up to Lu), or in other words they decrease at the lowering of ionic radius of the replacing rare earth. In particular, in inorganic phosphates this is observed in $RE(PO_4)$ synthetic monazites (*RE* = La, Ce, Pr, Nd, Sm, Eu, Gd) and xenotimes (*RE* = Tb, Dy, Ho, Er, Tm, Yb, Lu) [27], in $KLn(P_2O_7)\cdot2H_2O$ diphosphates (*Ln* = Gd, Tb, Yb) [28], and in hybrid diphosphates $Ln_2(NH_2(CH_2)_2NH_2)_2(HP_2O_7)_2\cdot4H_2O$ (*Ln* = Eu, Tb, Er) [29]. In particular, for what concerns the present work, we will discuss

X-ray powder structures, and thus unit cell parameters and bond lengths herein, coming from Rietveld refinements of available $Ca_9RE(PO_4)_7$ structures in the literature [6,30–32].

Interpretation of unit cell (u.c.) parameters reported for La-, Pr-, Nd-, Eu-, Gd-, Dy-, Tm-, Yb- [6], Ce- [30], Lu- [31], Tb-, and Ho- phases [32] shows a decreasing trend in the refined unit cell parameter values, ranging from $a = b = 10.4695(3)$ Å, $c = 37.500(3)$ Å (La) to $a = b = 10.4164(1)$, $c = 37.302(1)$ Å (Lu). The same trend is followed by the cell volumes: from 3559.7(2) (La) to 3505.1(1) Å^3 (Lu), while, as a consequence, the calculated density increases from 3.25 Mg·m^{-3} (La) up to 3.41 Mg·m^{-3} (Lu). Generally, only some small deviations are observed for such trends, as in the case of the Tb and Ho phase in the a parameter, or for Lu in a, c, and V parameters. Figure 2 reports u.c. parameters for available $Ca_9RE^{3+}(PO_4)_7$ structures, plotted as a function of RE ionic radius; in particular Figure 2a reports the a parameter, Figure 2b reports the c parameter, and Figure 2c depicts the volume trend.
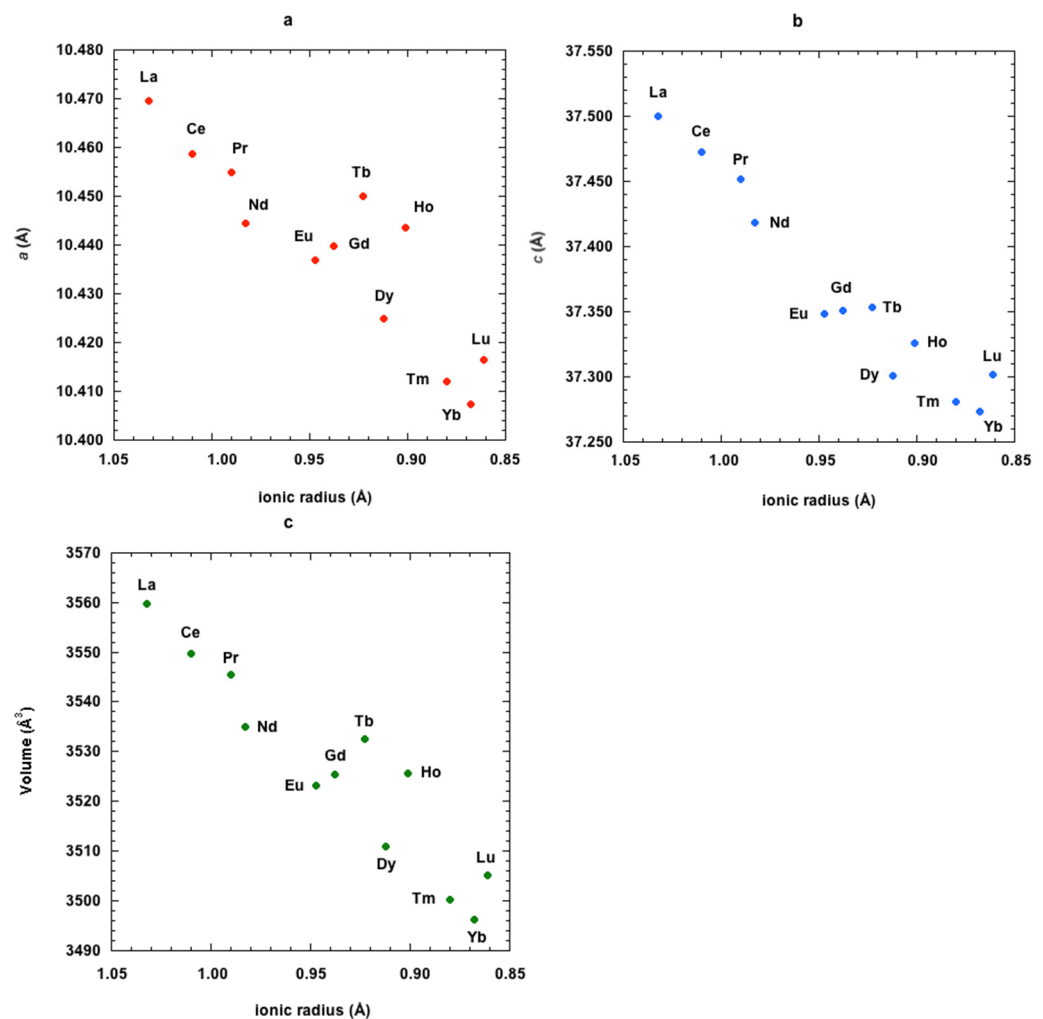
Figure 2. Unit cell parameters of RE β–TCP as a function of RE ionic radius (for 6-folded polyhedra). (**a**) a parameter (Å); (**b**) c parameter (Å); (**c**) Volume (Å^3). Data from [6], except Ce [30], Lu [31], Tb and Ho [32].

For better describing the $Ca_9RE^{3+}(PO_4)_7$ structure, the site notation proposed by Yashima et al. (2003) [20] in the neutron refinement model of β-TCP will be adopted across the work. Thus, five cationic sites are present in the structures, three in a general position (Wyckoff notation 18*b*) named M1, M2, and M3 sites, and two in a special position (6*a*), named M4 and M5. The M4 site is only partially occupied, being in β–TCP the site occupancy factor usually fixed at 1/2 for allowing the charge balance [20]. Two phosphorous and nine oxygen atoms are located on general positions, while a third phosphorous atom

and the O10 atom are placed on special positions (*6a*). The coordination environments of the single M1–M5 sites are usually respected in β–TCP structures. M1 displays irregular 7-fold coordination, while M2 and M3 display irregular 8-fold coordination, according to a Ca-O bonding sphere fixed at about 2.81 Å. M5 shows a fairly regular octahedral geometry, and M4 presents an uncommon triangular coordination, with three oxygen atoms related for symmetry.

In the isotypic mineral whitlockite, despite the presence of Mg^{2+} replacing Ca^{2+} at the M5 octahedral site, there are no substantial modifications in number and coordination of sites [22]. Eventually, M4 coordination number possibly increases up to six, due to a second group of three oxygen atoms related for symmetry found over 2.81 Å [22], providing very weak contributions in terms of valence bonds [33].

In $Ca_9RE^{3+}(PO_4)_7$ compounds, as for the case of present samples reported in this work, the most important structural modification compared to pure β–TCP and natural whitlockite is the M4 site resulting completely vacant, insofar as $6RE^{3+}$ and three vacancies have been substituted for $9Ca^{2+}$. The *RE* atoms are usually spread over three of the four remaining sites: in M1, M2, and M3, while M5 is fully occupied by Ca, according to [13], or in M1, M2, and M5 sites according to [31] as described later.

(PO_4) groups in $Ca_9RE^{3+}(PO_4)_7$ compounds show tetrahedral coordination, which in most cases is quite regular, with P-O bond distances ranging between 1.43(4) (La) and 1.57(4) (Pr) Å for a $P(1)O_4$ tetrahedron, 1.23(6) and 1.74(6) Å (both in Yb phase) for $P(2)O_4$, and 1.43(5) (La) and 1.71(8) Å (Yb) for $P(3)O_4$, in good agreement with P-O bond values found for orthophosphate phases [34], even if some short P-O distances are observed in phosphate structural refinements from powder X-ray data [29,35], when compared with those observed from single-crystal X-ray data, they are usually not lower than 1.40 Å [34,36,37].

Ca and mixed Ca/*RE* cations are involved in complex coordinations: $M1O_8$, $M2O_7$, $M3O_8$, fixing the threshold M-O at 2.81 Å; the last cationic site is occupied by a fairly regular octahedron $M5O_6$ (Figure 3), owing to the site symmetry, which produces two terns of distances. Bond distances in different sites range between 2.28(8) (Tm) and 2.81(8) (Dy) Å for the M1 site, 2.21(10) (Eu) and 2.57(6) Å (Yb) for the M2 site, 2.29(8) (Gd) and 2.79(5) (Yb) for the M3 site, and 2.20(6) (Dy) and 2.38(6) (La) for the M5 site [31]. In addition, the average M-O values, reported in [6,31,32], show that bond distances are quite homogeneous among M1, M2, and M3 sites, while decreasing in the M5 site, for packing reasons. In a recent structural study on $Ca_9Tb(PO_4)_7$ TCP [32], the $M2O_8$ polyhedron is described as 7-fold coordinated by excluding the longest M2-O distance. In these compounds the possibility that a longer bond may change in an interaction is not unlikely, and the problem should be considered from a bond valence perspective [33], according to the single bond length values.
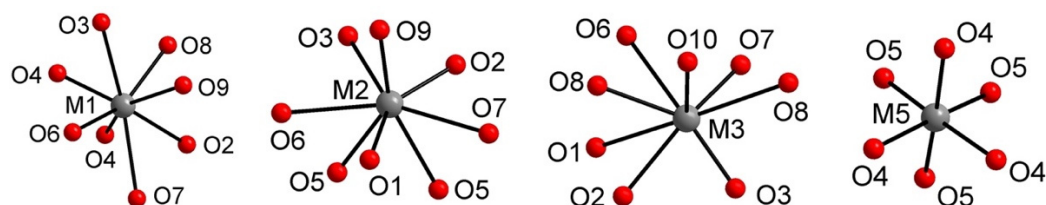
Figure 3. Polyhedral environment in structural sites of $Ca_9RE^{3+}(PO_4)_7$ β–TCP.

The rare-earth distribution within such compounds can occur with two different mechanisms: (1) *RE* in M1, M2, and M3 sites, with no occurrence in M5 [13]; (2) *RE* in M1, M2, and M5 sites, but not in M3 [6]. Analysis of the structure of available $Ca_9RE(PO_4)_7$ highlights that *RE* = La, Pr, Nd, Eu, Gd, Tb, and Dy enter sites M1, M2, and M3, and not site M5 for steric reasons due to the large *RE* ionic radius. Conversely, Ho, Tm, Yb, and Lu prefer the second mechanism, entering site M5 over M1 and M2 sites, and not M3, because of their lower ionic radius, giving results that are quite comparable to that of Ca^{2+},

1.00 Å [38], in the 6-coordinated M5 site. The *RE* distribution in β-TCP within single M sites as a function of the atomic number, observed for most of *RE* comprised among La and Lu, is reported in [31,32]. In M1, the distribution initially increases for all *RE* from La^{3+} up to Ho^{3+}, with a small deviation for the Tb-phase, and afterwards decreases in Tm, Yb, and Lu. In M2 a fairly irregular distribution occurs, increasing from La up to Tb; afterwards it decreases with deviations in Tm and Lu terms. In M3, the trend is regularly decreasing, becoming null in Ho, Tm, Yb, and Lu. Finally, in the M5 site, the *RE* does not occur for all phases up to Dy, except in the same phases that resulted in the M3 site being *RE*-free. The only deviation in those trends is represented by the Ce phase [30], where the *RE* dopant is fully refined in the M5 site. The *RE* distribution trends in β-TCP are reported in Figure 4.
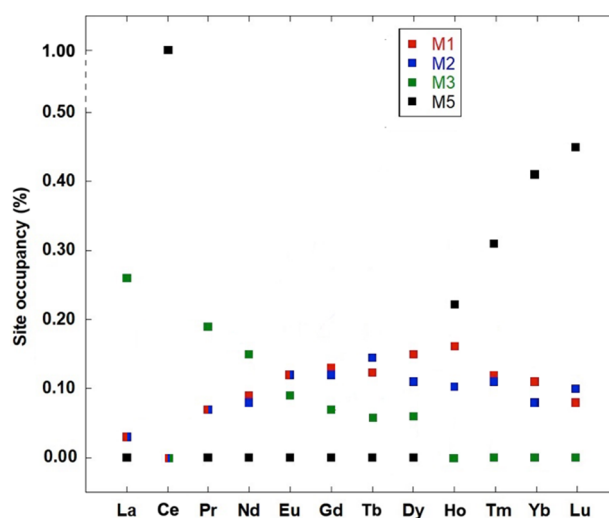

Figure 4. Distribution of *RE* cations within M1, M2, M3, and M5 sites in available $Ca_9RE(PO_4)_7$ structure refinements; data from [6], with the exception of Ce [30], Tb and Ho [32], and Lu [31].

3.1.4. Three-Dimensional Framework

The three-dimensional framework in $Ca_9RE(PO_4)_7$ materials can be described as the repetition of two columnar arrays, indicated as 'A' and 'B', down the *c*-axis (Figure 5). The A array is made by the sequence of . . . $P1O_4$ $M5O_6$ $P1O_4$ . . . polyhedra, while the B array displays the . . . $P3O_4$ $M1O_8$ $M3O_8$ $M2O_8$ $P2O_4$ $P3O_4$ . . . . polyhedra repetition (Figure 5). The A array does not display sharing oxygen atoms among $P1O_4$ and $M5O_6$ groups. On the contrary, in the B array the single polyhedra are joined to each other via vertices or edges, i.e., the $P2O_4$ group and $M2O_8$ polyhedron share the O1 vertex, $M2O_8$ and $M3O_8$ polyhedra share the O9-O3 edge, and $M3O_8$ and M1-O8 polyhedra share the O6-O7 edge, while $M1O_8$ is joined with the $P3O_4$ group through the O8 vertex (inset b of Figure 5). In some phases of the series, for example $Ca_9Tb(PO_4)_7$, owing to the lack of the Ca3-O9 bond, the $M2O_8$-$M3O_8$ polyhedral sharing is described simply as O3 vertex sharing. Each A array is surrounded by six B columns, while each B column is surrounded by two A and four B columns (Figure 6).

The two arrays are joined among themselves via different mechanisms; the most important is that formed by the $M5O_6$ octahedron through corner-sharing with P2 and P3 tetrahedra, the $[M5(PO_4)_6]$ unit, depicted in Figure 5 (inset b). Such units assure the link between one A column and six B columns, being flat in the *c* direction and holding 6 different tetrahedra belonging to as many as B columnar arrays (Figure 6). Another important joining network among A and B arrays, in present $Ca_9RE(PO_4)_7$ structures, is that formed by the $P1O_4$ group, forced from site symmetry of P1 (*6a* site). The $P1O_4$ tetrahedron can be described as a regular triangular pyramid, whose three base-vertices are the three O9 atoms, which in turn belong simultaneously to one $M1O_8$ from an adjacent B array (inset a of Figure 6), and to $M2O_8$ and $M3O_8$ polyhedra belonging to another B array. Owing again to the site symmetry, the joining mechanism is repeated three times,

further helped by the O10 apical vertex of the P1O$_4$ tetrahedron, which is joined to three M3O$_8$ groups (inset (a) of Figure 6).
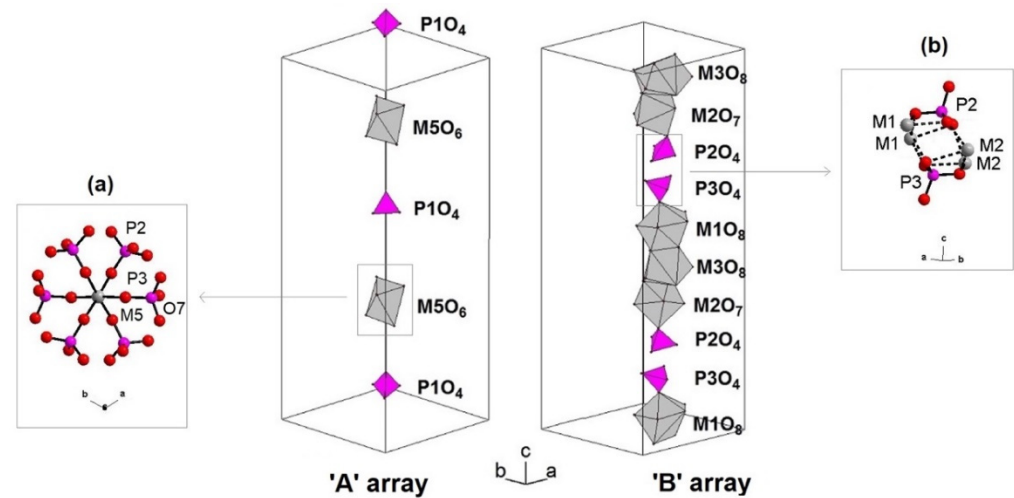
Figure 5. Ca$_9$*RE*(PO$_4$)$_7$ packing: A and B arrays. Inset (**a**): detail of [M5(PO$_4$)$_6$] unit. Inset (**b**): joining mechanism among B arrays (M-O bonds dashed).
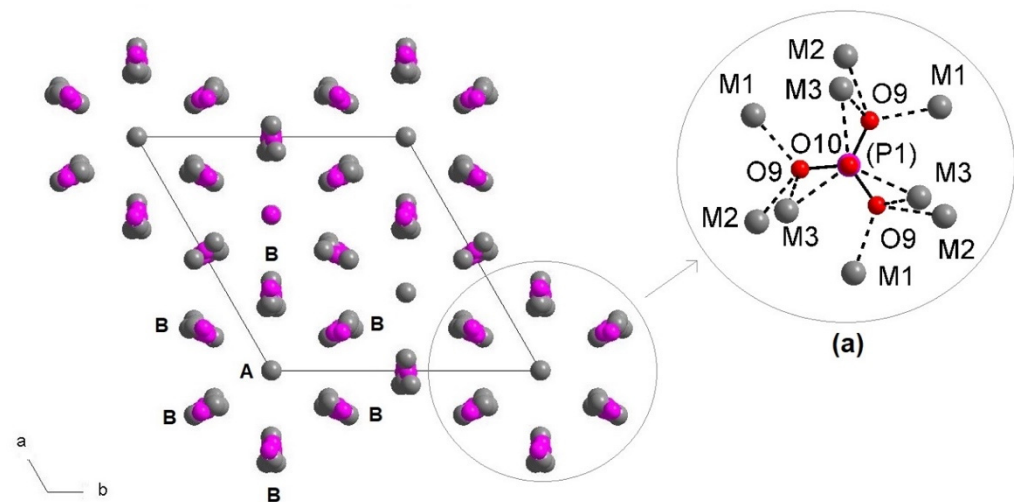

Figure 6. View down *c* of the *RE* β–TCP framework. Inset (**a**): (P1O$_4$) group environment and joining mechanisms with M1-M2-M3 polyhedra from adjacent B arrays.

3.2. FTIR Spectroscopy

The infrared features of the studied compounds in the 1600–400 cm^{-1} region (Figure 7) are consistent with the ones observed for pure β-TCP [6]. The phosphate ion has four vibrational modes active in the infrared, compatible with a C$_1$ symmetry: the symmetric stretching ν_1, the symmetric double degenerate bending mode ν_2, and the triple degenerate asymmetric stretching (ν_3) and asymmetric bending (ν_4) modes [6]. The substitution of *RE* in Ca sites in the studied compounds only causes an increase in multiplicity, accompanied by a shift in some of the band positions dependent of the ionic radius of the *RE* [6,31]. The most intense ν_3 peak is, for example, slightly shifted to lower wavenumbers from Dy to Nd as the ionic radius increases (from 1033 cm^{-1} to 1029 cm^{-1} to 1027 cm^{-1} for Ca$_9$Dy(PO$_4$)$_7$, Ca$_9$Gd(PO$_4$)$_7$, and Ca$_9$Nd(PO$_4$)$_7$, respectively) [6,31]. All the samples show the most intense group of components in the 1000–1200 cm^{-1} region, corresponding to antisymmetric stretching ν_3 (P-O). The bands between 1000 and 900 cm^{-1} can be assigned to the symmetric stretching bands ν_1 (P-O). The bending modes are located at lower wavenumbers. Two intense bands at about 610 cm^{-1} (609 for Dy- and Gd-based materials, 607 for Nd) and 551 cm^{-1} for all the samples are attributable to the O-P-O

antisymmetric bending. The symmetric bending mode ν_2 $(PO_4)^{3-}$ appears as a weak component around 440 cm^{-1}.
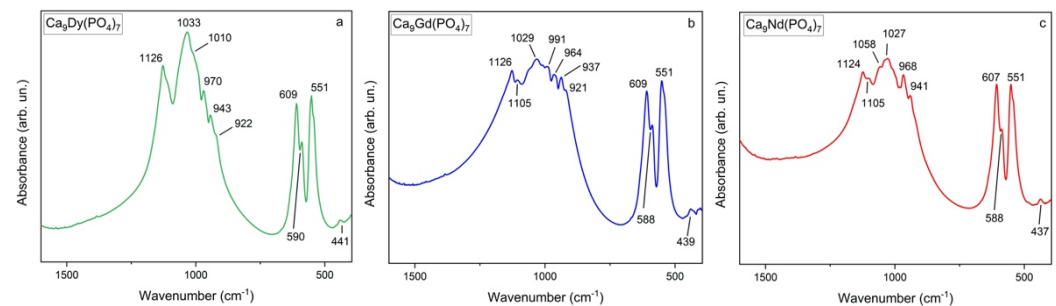
**Figure 7.** FTIR spectra of (**a**) $Ca_9Dy(PO_4)_7$, (**b**) $Ca_9Gd(PO_4)_7$, and (**c**) $Ca_9Nd(PO_4)_7$ in the 1600–400 cm^{-1} region.

3.3. Photoluminescence Spectroscopy

3.3.1. Dy^{3+} TCP

As shown in Figure 8a, many bands are present in the excitation spectrum of $Ca_9Dy(PO_4)_7$ by monitoring the emission at the most intense emission band (571 nm, $^4F_{9/2} \rightarrow {}^6H_{13/2}$). The spectral features can be attributed to absorption transitions from the ground state $^6H_{15/2}$ to $^4H_{13/2} + {}^4G_{9/2}$ (294 + 299 nm), $^6P_{3/2}$ (324 nm), $^4F_{5/2} + {}^4I_{9/2}$ (337 nm), $^4M_{15/2} + {}^6P_{7/2} + {}^4I_{11/2}$ (350 nm), $^4M_{19/2} + {}^6P_{5/2} + {}^4P_{3/2}$ (364 nm), $^4F_{7/2} + {}^4I_{13/2} + {}^4M_{21/2} + {}^4K_{17/2}$, (387 nm), $^4G_{11/2}$ (426 nm), $^4I_{15/2}$ (452 nm), $^4F_{9/2}$ (472 nm) [8,39,40]. Among them, $^6H_{15/2} \rightarrow {}^4M_{15/2} + {}^6P_{7/2} + {}^4I_{11/2}$ is the most intense one.
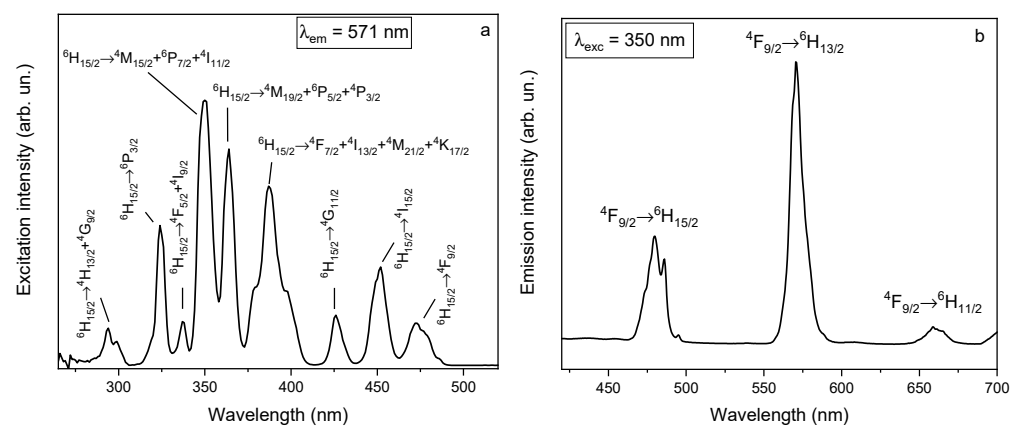
Figure 8. Excitation (**a**) and emission (**b**) spectra of $Ca_9Dy(PO_4)_7$.

No CT bands are observed in the excitation spectrum, in agreement with previous reports [9].

Excitation at 350 nm brings the Dy^{3+} ion to the $^6P_{7/2}$ level, and that is followed by non-radiative relaxation to the $^4F_{9/2}$ level [41]. Thus, the visible emission spectrum upon excitation at 350 nm shows three main components around 480 nm, 570 nm, and 660 nm (Figure 8b), belonging to 4f-4f intraconfigurational transitions of Dy^{3+} [9]. They correspond to $^4F_{9/2} \rightarrow {}^6H_{15/2}$ (blue), $^6H_{13/2}$ (yellow), and $^6H_{11/2}$ (red) [42]. The observed features are rather broad and do not show a well-resolved Stark structure. This indicates that in the material under investigation the sites accommodating the dopant ion are affected by disorder.

No significant emission is detected around 400 nm, deriving from levels lying higher in energy than $^4F_{9/2}$. This indicates that thermal population of these high energy levels ($^4H_{15/2}$ and above) can be neglected. The strongest emission band ($^4F_{9/2} \rightarrow {}^6H_{13/2}$), located in the yellow region, is of forced electric dipole nature ($|\Delta J| = 2$) and is therefore sensitive

to the surronding environment, whilst the $^4F_{9/2} \rightarrow {}^6H_{15/2}$ (blue region) is of magnetic dipole nature ($|\Delta J| = 1$) and its intensity does not depend on the host [8,40,41].

The dominance of the yellow band above the blue one is compatible with a low-symmetry site for Dy^{3+} without an inversion center [40,41].
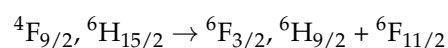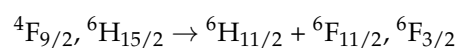
The asymmetry ratio is defined as the ratio between the integrated emission intensity of the yellow to the blue bands and gives information about the local symmetry and the covalency of Dy^{3+} ions in a crystal [40]. For $Ca_9Dy(PO_4)_7$, a very high value of 2.18 was obtained, indicating that the dopant ions are accomodated in low-symmmetry sites, such as the ones available in the TCP structure [6,31]. The asymmetry ratio changes with Dy^{3+} concentration, which is related to structural changes in the local environment of this ion [9]. By varying the ratio between the yellow and blue components, it is possible to tune the final colour of the material, potentially obtaining white light [41]. The prevalence of the yellow component obtained upon excitation at 350 nm is shown in the CIE diagram (Figure 9a).
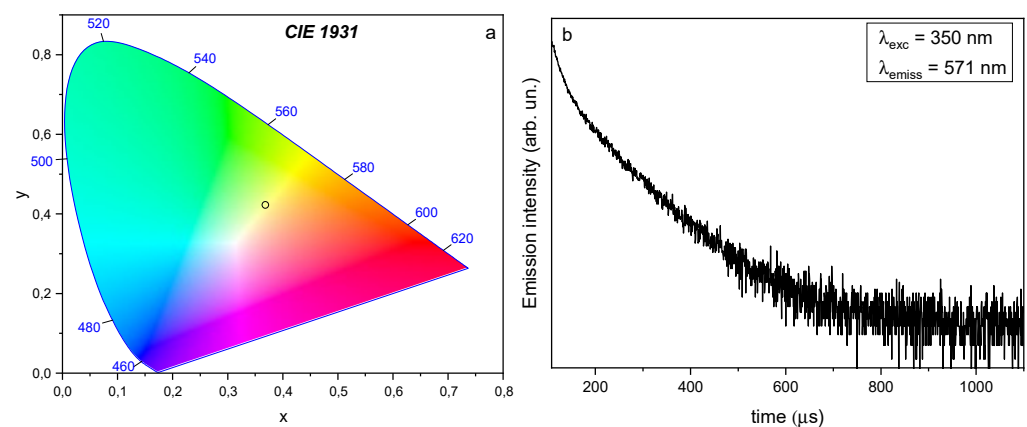
Figure 9. (**a**) CIE diagram for $Ca_9Dy(PO_4)_7$ material upon excitation at 350 nm. (**b**) Decay time obtained for the compound $Ca_9Dy(PO_4)_7$ upon excitation at 350 nm and by detecting the emission at 571 nm.

The decay curve of the $^4F_{9/2}$ level is non-exponential, with a short component of 19 μs and a long one of 97 μs (Figure 9b). This could indicate the presence of multiple emitting centers, such as two or more crystallographic sites occupied by the emitting species. This is in accordance with the presence of both Ca^{2+} and RE^{3+} in the same crystallographic sites [3] and with the occupancy of three of the four Ca-sites in $Ca_9Eu(PO_4)_7$ [13]. In particular, a preference for the 8-fold coordinated M1 and M2 sites for cations such as Eu^{3+} and Tb^{3+} was found in concentrated compounds [3]. These factors are both responsible for the disorder of the whitlockite structure. However, the non-exponential profile of the decay curve could also be ascribed to the presence of energy transfer processes, namely cross-relaxation, given the concentrated nature of the material under investigation.

The long component is definitely shorter compared to the values found in other matrices where Dy^{3+} is present as a dopant. To give some examples, the lifetime was found to be greater than 370 μs in $NaYF_4$ microcrystals [40], or ranging from 150 up to 1022 μs in glasses [3], then again 305 μs in Y_2O_3:Dy^{3+} nanophosphors [43]. Cross-relaxation between Dy^{3+} pairs to the intermediate levels Dy^{3+} ($^6F_{3/2}$) and Dy^{3+} ($^6H_{9/2}$) is probably responsible for the observed decrease in decay time compared to the values reported for different compounds [42,43]. The process is enhanced when the ions are in close proximity according to the distance-dependence of the resonant energy transfer mechanism [9]. The pathways involved in Dy^{3+}-doped materials are as follows [8]:

$$^4F_{9/2}, {}^6H_{15/2} \rightarrow {}^6H_{11/2} + {}^6F_{11/2}, {}^6F_{3/2}$$

$$^4F_{9/2}, {}^6H_{15/2} \rightarrow {}^6F_{3/2}, {}^6H_{9/2} + {}^6F_{11/2}$$

and usually lead to concentration quenching [43]. Nevertheless, besides the particular multisite distribution of cations, the shorter distance between *RE* dopants in the analogous Eu^{3+} compound is 3.67 Å, between M1 and M2 sites, which was found to be large enough to limit the $Eu^{3+} \rightarrow Eu^{3+}$ energy transfer [3,13]. Moreover, a deep study of decay behaviour of concentrated and diluted Tb^{3+} and Eu^{3+} ions in $Ca_9Eu(PO_4)_7$ and $Ca_9Tb(PO_4)_7$ demonstrated that for RE^{3+}-concentrated whitlockite materials, the energy migration between ions is not efficient due to the energy mismatch between the Stark levels in neighbouring sites, preventing concentration quenching [3]. Furthermore, while low doping concentrations usually give single exponential decays, non-exponential behaviour can be related to a high dopant concentration, due to an increase in ion–ion interactions and consequent non-radiative pathways [9]; indeed, $Ca_9Dy(PO_4)_7$ presents a different and intense luminescence and only partial quenching despite Dy^{3+} being a constituent of the matrix, confirming the low interaction between ions in whitlockites.

Due to the dependence of the site occupancy on the ion size, it is likely that the same structure-dependent luminescence behaviour occurs for Dy^{3+} and Gd^{3+}. This explains the intense emission as well as a lifetime in the 100-μs region of Dy^{3+} even as a full constituent in β-TCP, due to the similarity of this cation with the ones previously studied. This makes these materials very interesting for applications like thermoluminescence or phosphors [13].

3.3.2. Gd^{3+} TCP

The excitation spectrum of $Ca_9Gd(PO_4)_7$ (Figure 10a) shows 3 bands, at 36,630, 36,363, and 35,842 cm^{-1}, attributable to the transitions $^8S_{7/2} \rightarrow {}^6I_{11/2}$, $^8S_{7/2} \rightarrow {}^6I_{17/2}$, and $^8S_{7/2} \rightarrow {}^6I_{7/2}$, respectively [44].
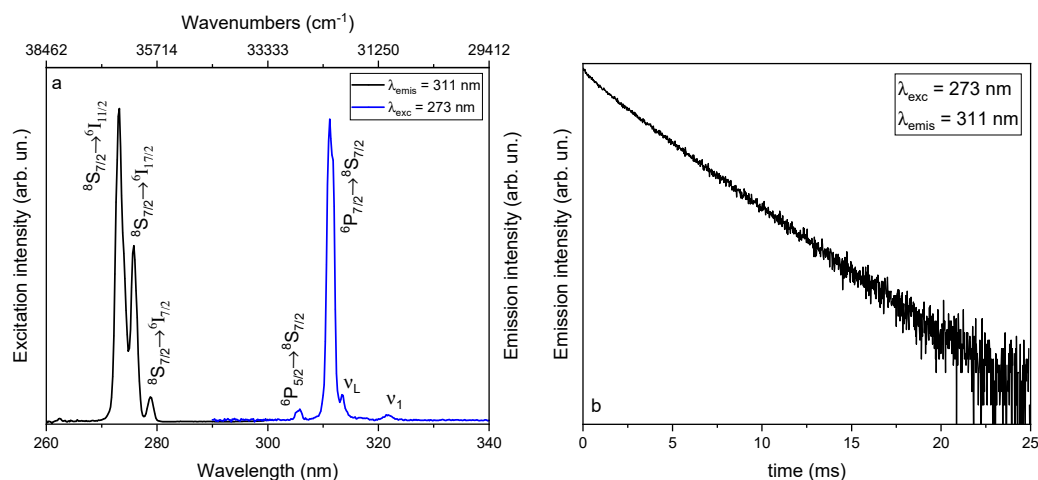
Figure 10. (**a**) Excitation spectrum of $Ca_9Gd(PO_4)_7$ (black line) at λ_{emis} = 311 nm. Emission spectrum of $Ca_9Gd(PO_4)_7$ (blue line) at λ_{exc} = 273 nm. (**b**) Decay time obtained for the compound $Ca_9Gd(PO_4)_7$ upon excitation at 273 nm and by detecting the emission at 311 nm.

The emission spectrum upon excitation at 273 nm is also shown in Figure 10a. The strongest band is located at 32,133 cm^{-1} and corresponds to the $^6P_{7/2} \rightarrow {}^8S_{7/2}$ transition, and in particular is the zero-phonon line [45]. For Gd^{3+}-based samples, vibronic lines may also be visible besides electronic transitions that are due to the interaction between 4f electrons of RE^{3+} and lattice vibrations [16]. These are due to electron–phonon coupling and have a strong influence on the spectroscopic features of a given material; for these reasons, they are important from the application point of view and they can give information about the local structure of rare-earth-based compounds [16]. These cooperative transitions involve electronic transitions on the metal together with vibrational transitions in the coordinating environment [46], with a consequent mixing of opposite parity wavefunctions [47]. This gives rise to Stokes and anti-Stokes structure in the emission spectrum [47]. Thus, in the emission spectrum of $Ca_9Gd(PO_4)_7$, vibronic features generated by the coupling of

the 4f electrons of the Gd^{3+} ion with lattice vibrations are visible close to the zero-phonon transition [45]. At energies higher than the $^6P_{7/2} \to {}^8S_{7/2}$ transition, only one band is observed at 32,679 cm^{-1}, corresponding to the thermally activated $^6P_{5/2} \to {}^8S_{7/2}$ transition [45,46]. Two vibronic peaks at 31,908 and 31,094 cm^{-1} are present at lower energies with respect to the most intense band (located at 32,133 cm^{-1}) and are characterized by a broad shape and a low intensity [45]. The band at 31,908 cm^{-1} is 225 cm^{-1} distant from the main peak, thus it is presumably associated with lattice vibrations (indicated as ν_L in Figure 10a). Indeed, the peak located at 31,094 cm^{-1} is 1039 cm^{-1} shifted with respect to the zero-phonon line, a value close to the peak located at 1029 cm^{-1} in the FTIR spectrum of $Ca_9Gd(PO_4)_7$ (Figure 7b) corresponding to the symmetric stretching bands ν_1 (P-O) (this band is indicated as ν_1 in Figure 10a). The band located at 32,679 cm^{-1} is 546 cm^{-1} from the 0-0 line (32,133 cm^{-1}) and is also compatible with the O-P-O antisymmetric bending at 551 cm^{-1} in the FTIR spectrum of $Ca_9Gd(PO_4)_7$ reported in Figure 7b.

Moreover, the zero-phonon line presents a not-resolved shoulder at 32,072 cm^{-1} that probably belongs to the first coordination sphere, while the lower energy peaks are related to the second coordination sphere [45]. The integrated intensity of the second coordination sphere vibronic bands is 0.5% of the main transition, several times lower than the bands associated with the first coordination sphere [45]. In the $Ca_9Gd(PO_4)_7$ sample, the integrated area of $^6P_{7/2} \to {}^8S_{7/2} + \nu$ vibronic peaks is lower than 7% with respect to the zero-phonon line, comparable with those found for Gd in other matrices [16,48].

The decay curve of the $^6P_{7/2}$ level, measured by observing in the zero-phonon band, is mono-exponential, characterized by a lifetime of 3.24 ms (Figure 10b). This value, together with the high intensity of Gd^{3+} emission, indicates that concentration quenching due to energy migration among the Gd^{3+} ions is negligible [48]. The lifetime value for Gd-based whitlockite is similar to that found in LaB_3O_6:Gd^{3+} glass and crystal [16]. This corresponds to a decay rate constant of 308.6 s^{-1}, close the value found for the estimated radiative rate of Gd^{3+} in a site without inversion symmetry [46]. This may suggest that non-radiative transitions are almost absent in the present material. Similar values are also found at low temperature for Gd-doped $LaAlO_3$, where the zero-phonon transition probability has been determined to be 297 s^{-1}, and the lifetime for the same compound is 3.6 ms [47].

3.3.3. Nd^{3+} TCP

The $Ca_9Nd(PO_4)_7$ compound shows emission in the NIR region upon excitation at 520 nm. In detail, upon excitation in the $^4I_{9/2} \to {}^4G_{9/2} + {}^4G_{7/2} + {}^2K_{13/2}$ [49], splitted but weakly resolved emission bands appear around 900 nm, 1050 nm, and 1330 nm, corresponding to $^4F_{3/2} \to {}^4I_{9/2}$, $^4F_{3/2} \to {}^4I_{11/2}$ and $^4F_{3/2} \to {}^4I_{13/2}$, respectively (Figure 11). The probability of spontaneous emission from these transitions is dependent on the ratio between the Judd–Ofelt parameters Ω_4 and Ω_6, namely the spectroscopic quality factor $X = \Omega_4/\Omega_6$. In the present material, the $^4F_{3/2} \to {}^4I_{11/2}$ transition is dominating, as usually occurs when X is <1.15 [50]. A value in this region was found for Nd^{3+} in alkali chloroborophosphate glasses [51] and in tetraborate glasses [50] and the lower the value, the higher the intensity for laser applications. Due to the available equipment, and to the poor crystallinity of the samples, it was not possible to collect the excitation spectrum, or to perform the lifetime analysis.
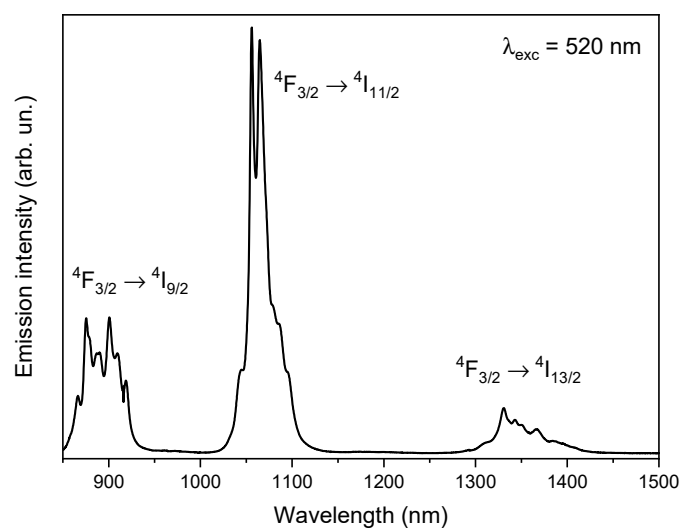
Figure 11. Emission spectrum of $Ca_9Nd(PO_4)_7$ at $\lambda_{exc} = 520$ nm.

4. Conclusions

Microcrystalline $Ca_9RE(PO_4)_7$ (RE = Nd, Gd, Dy) phosphor materials were prepared by solid state reaction at T = 1200°. The work aimed to study possible applications of such RE-TCP by coupling the structural information with experimental results of photoluminescence analysis. According to previous structural investigations, distribution of rare-earth dopants in structural sites of $Ca_9RE(PO_4)_7$ matrices is well known: for lowering of the RE ionic radius, in $Ca_9RE(PO_4)_7$ phosphates the RE ratio regularly increases in M1 and M2 for all phases up to the Tb term, from which both the trends slightly decrease, while in M3 the RE ratio decreases, even being null in the last 4 terms; last, the RE ratio in M5, the octahedral site with higher symmetry, is null for all phases up to Dy, after which the site starts to fill.

The PL emission spectra confirmed, for Dy^{3+} and Gd^{3+} phases, the presence of dopants in the framework in a low-symmetry site with some local structural disorder, which still allows the presence of vibrational features. For the Nd^{3+} phase, the location of RE dopant in the sites was not achieved, due to the lack of excitation spectrum and lifetime analysis due to the instrumental limitations and poor quality of the microcrystals. These materials showed strong and well resolved luminescence spectra although the emitting RE^{3+} was present as a bulk constituent, suggesting that energy migration between the luminescent centers is minimal. These samples are also interesting as examples of materials emitting in three different regions of the spectra: UV (Gd^{3+}), visible (yellow) (Dy^{3+}), and NIR (Nd^{3+}).

Author Contributions: V.P., M.B. and F.C. conceived and designed the main ideas together, and wrote and supervised the whole work; A.E.K. synthesized the samples and collected XRD data; F.C. and D.M.T. contributed to the TCP structural description; V.P. contributed in luminescence and FTIR spectroscopies. All authors have read and agreed to the published version of the manuscript.

Data Availability Statement: Fractional atomic coordinates and isotropic displacement parameters from structure solutions of the title compounds can be obtained from the Inorganic Crystal Structuure Database (ICSD, Fachinformationszentrum Karlsruhe, 76344 Eggenstein-Leopoldshafen, Germany, (Fax: +49-7247-808-666; e-mail: crysdata@fiz-karlsruhe.de) [34]) on quoting the following depository numbers CSD432796 (Nd-TCP), CSD432793 (Gd-TCP), and CSD432791 (Dy-TCP). XRD spectra were deposited at the PDF-2 (Powder Diffraction File-2) database of International Center for Diffraction Data (ICDD, Newton Square, PA, USA, 2003 [25]) with card numbers 00-070-0125 (Nd-TCP), 00-070-0127 (Gd-TCP), and 00-070-0128 (Dy-TCP).

References

1. Trevisani, M.; Ivanovskikh, K.V.; Piccinelli, F.; Speghini, A.; Bettinelli, M. Fast UV luminescence of Pr^{3+}-doped calcium lutetium whitlockite. *ECS Trans.* **2012**, *41*, 11–17. [CrossRef]

2. Piccinelli, F.; Trevisani, M.; Plaisier, J.R.; Bettinelli, M. Structural study of Yb^{3+}, Eu^{3+} and Pr^{3+} doped $Ca_9Lu(PO_4)_7$. *J. Rare Earth* **2015**, *33*, 977–982. [CrossRef]

3. Carrasco, I.; Piccinelli, F.; Bettinelli, M. Optical spectroscopy of $Ca_9Tb_{1-x}Eu_x(PO_4)_7$ (x = 0, 0.1, 1): Weak donor energy migration in the whitlockite structure. *J. Phys. Chem. C.* **2017**, *121*, 16943–16950. [CrossRef]

4. Trevisani, M.; Ivanovskikh, K.V.; Piccinelli, F.; Speghini, A.; Bettinelli, M. Interconfigurational 5d→4f luminescence of Ce^{3+} and Pr^{3+} in $Ca_9Lu(PO_4)_7$. *J. Phys. Condens. Matter* **2012**, *24*, 385502. [CrossRef]

5. Watras, A.; Carrasco, I.; Pazik, R.; Wiglusz, R.J.; Piccinelli, F.; Bettinelli, M.; Deren, P.J. Structural and spectroscopic features of $Ca_9M(PO_4)_7$ (M = Al^{3+}, Lu^{3+}) whitlockites doped with Pr^{3+} ions. *J. Alloy. Compd.* **2016**, *672*, 45–51. [CrossRef]

6. El Khouri, A.; Elaatmani, M.; Della Ventura, G.; Sodo, A.; Rizzi, R.; Rossi, M.; Capitelli, F. Synthesis, structure refinement and vibrational spectroscopy of new rare-earth tricalcium phosphates $Ca_9RE(PO_4)_7$ (*RE* = La, Pr, Nd, Eu, Gd, Dy, Tm, Yb). *Ceram. Int.* **2017**, *43*, 15645–15653. [CrossRef]

7. Dikhtyar, Y.Y.; Deyneko, D.V.; Boldyrev, K.N.; Borovikova, E.Y.; Lipatiev, A.S.; Stefanovich, S.Y.; Lazoryak, B.I. Luminescent properties of Er^{3+} in centrosymmetric and acentric phosphates $Ca_8Mer(PO_4)_7$ (M = Ca, Mg, Zn) and $Ca_{9-x}Zn_xLa(PO_4)_7$:Er^{3+}. *Mater. Res. Bull.* **2021**, *138*, 111244. [CrossRef]

8. Lira, A.; Speghini, A.; Camarillo, E.; Bettinelli, M.; Caldiño, U. Spectroscopic evaluation of $Zn(PO_3)_2$:Dy^{3+} glass as an active medium for solid state yellow laser. *Opt. Mater.* **2014**, *38*, 188–192.

9. Chemingui, S.; Ferhi, M.; Horchani-Naifer, K.; Ferid, M. Synthesis and luminescence characteristics of Dy^{3+} doped $KLa(PO_3)_4$. *J. Lumin.* **2015**, *166*, 82–87. [CrossRef]

10. Kim, E.J.; Choi, S.W.; Hong, S.H. Synthesis and photoluminescence properties of Eu^{3+}-doped calcium phosphates. *J. Am. Ceram. Soc.* **2007**, *90*, 2795–2798. [CrossRef]

11. Malik, C.; Kaur, N.; Singh, B.; Pandey, A. Luminescence properties of tricalcium phosphate doped with dysprosium. *Appl. Radiat. Isot.* **2020**, *158*, 109062. [CrossRef] [PubMed]

12. Madhukumar, K.; Varma, H.K.; Komath, M.; Elias, T.S.; Padmanabhan, V.; Nair, C.M.H. Photoluminescence and thermoluminescence properties of tricalcium phosphate phosphors doped with dysprosium and europium. *Bull. Mater. Sci.* **2007**, *30*, 527–534. [CrossRef]

13. Ait Benhamou, R.; Bessière, A.; Wallez, G.; Viana, B.; Elaatmani, M.; Daoud, M.; Zegzouti, A. New insight in the structure—Luminescence relationships of $Ca_9Eu(PO_4)_7$. *J. Sol. State Chem.* **2009**, *182*, 2319–2325. [CrossRef]

14. Meenambal, R.; Nandha Kumar, P.; Poojar, P.; Geethanath, S.; Kannan, S. Simultaneous substitutions of Gd^{3+} and Dy^{3+} in β-$Ca_3(PO_4)_2$ as a potential multifunctional bio-probe. *Mater. Des.* **2017**, *120*, 336–344. [CrossRef]

15. Meenambal, R.; Poojar, P.; Geethanath, S.; Kannan, S. Structural insights in Dy^{3+}-doped β-Tricalcium phosphate and its multimodal imaging characteristics. *J. Am. Ceram. Soc.* **2017**, *100*, 1831–1841. [CrossRef]

16. Ellens, A.; Salemink, B.; Meijerink, A.; Blasse, G. Study of the vibronic transitions of Gd^{3+} and Eu^{3+} in crystalline materials and glasses of the same composition. *J. Sol. State Chem.* **1998**, *136*, 206–209. [CrossRef]

17. Sola, D.; Balda, R.; Peña, J.; Fernández, J. Site-selective laser spectroscopy of Nd^{3+} ions in 0.8$CaSiO_3$-0.2$Ca_3(PO_4)_2$ biocompatible eutectic glass-ceramics. *Opt. Express* **2012**, *20*, 10701–10711. [CrossRef] [PubMed]

18. Lecointre, A.; Bessière, A.; Viana, B.; Aït Benhamou, R.; Gourier, D. Thermally stimulated luminescence of $Ca_3(PO_4)_2$ and $Ca_9Ln(PO_4)_7$ (Ln = Pr, Eu, Tb, Dy, Ho, Er, Lu). *Radiat. Meas.* **2010**, *45*, 273–276. [CrossRef]

19. *Horiba Jobin Yvon DAS6 Fluorescence Decay Analysis Software User Guide*, version 2744.F.; Horiba Jobin Yvon SAS: Edison, NJ, USA, 2008; pp. 29–31.

20. Yashima, M.; Sakai, A.; Kamiyama, T.; Hoshikawa, A. Crystal structure analysis of β-tricalcium phosphate $Ca_3(PO_4)_2$ by neutron powder diffraction. *J. Sol. State Chem.* **2003**, *175*, 272–277. [CrossRef]

21. Mathew, M.; Schroeder, L.W.; Dickens, B.; Brown, W.E. Crystal Structure of α-$Ca_3(PO_4)_2$. *Acta Crystallogr. B* **1977**, *33*, 1325–1333. [CrossRef]

22. Capitelli, F.; Bosi, F.; Capelli, S.; Radica, F.; Della Ventura, G. Neutron and XRD single-crystal diffraction study and vibrational properties of whitlockite, the natural counterpart of synthetic tricalcium phosphate. *Crystals* **2021**, *11*, 225. [CrossRef]

23. Zhai, S.; Kanzaki, M.; Katsura, T.; Ito, E. Synthesis and characterization of strontium-calcium phosphate γ-$Ca_{3-x}Sr_x(PO_4)_2$ (0 ≤ x ≤ 2). *Mater. Chem. Phys.* **2010**, *120*, 348–350. [CrossRef]

24. Xie, X.D.; Gu, X.P.; Chen, M. An occurrence of tuite, gamma-$Ca_3(PO_4)_2$, partly transformed from Ca-phosphates in the Suizhou meteorite. *Meteorit. Planet. Sci.* **2016**, *51*, 195–202. [CrossRef]

25. *The Powder Diffraction File*; International Center for Diffraction Data: Newton Square, PA, USA, 2003.

26. Spedding, F.H. *Lanthanide Contraction*; McGraw-Hill Education: New York, NY, USA, 2020.

27. Ni, Y.-X.; Hughes, J.M.; Mariano, A.N. Crystal chemistry of the monazite and xenotime structures. *Am. Mineral.* **1995**, *80*, 21–26. [CrossRef]

28. Tahiri, A.A.; El Bali, B.; Lachkar, M.; Piniella, J.F.; Capitelli, F. Crystal structure of new lanthanide diphosphates $KLnP_2O_7 \cdot 2(H_2O)$ (Ln = Gd, Tb, Yb). *Z. Kristallogr.* **2006**, *221*, 173–177. [CrossRef]

29. Capitelli, F.; El Bali, B.; Essehli, R.; Lachkar, M.; Da Silva, I. New hybrid diphosphates $Ln_2(NH_2(CH_2)_2NH_2)_2(HP_2O_7)_2 \cdot 4H_2O$ (Ln = Eu, Tb, Er): Synthesis, single crystal and powder X-ray crystal structure. *Z. Kristallogr.* **2006**, *221*, 788–794. [CrossRef]

30. Zhang, S.; Li, Y.; Lv, Y.; Fan, L.; Hu, Y.; He, M. A full-color emitting phosphor $Ca_9Ce(PO_4)_7:Mn^{2+}$, Tb^{3+}: Efficient energy transfer, stable thermal stability and high quantum efficiency. *Chem. Eng. J.* **2017**, *322*, 314–327. [CrossRef]

31. Capitelli, F.; Rossi, M.; El Khouri, A.; Elaatmani, M.; Corriero, N.; Sodo, A.; Della Ventura, G. Synthesis, structural model and vibrational spectroscopy of lutetium tricalcium phosphate $Ca_9Lu(PO_4)_7$. *J. Rare Earths* **2018**, *36*, 1162–1168. [CrossRef]

32. Rizzi, R.; Capitelli, F.; Lazoryak, B.I.; Morozov, V.A.; Piccinelli, F.; Altomare, A. A comprehensive study on $Ca_9Tb(PO_4)_7$ and $Ca_9Ho(PO_4)_7$ doped β-tricalcium phosphates: Ab-initio crystal structure solution, Rietveld analysis and dielectric properties. *Cryst. Growth Des.* **2021**, *21*, 2263–2276. [CrossRef]

33. Brown, I.D.; Altermatt, D. Bond-valence parameters obtained from a systematic analysis of the Inorganic Crystal Structure Database. *Acta Crystallogr. B* **1985**, *41*, 244–247. [CrossRef]

34. *Inorganic Crystal Structure Database (ICSD)*, version 2018–2; Fachinformationszentrum: Karlsruhe, Germany, 2018.

35. El Bali, B.; Capitelli, F.; Alaoui, A.T.; Lachkar, M.; da Silva, I.; Alvarez-Larena, A.; Piniella, J.F. New thallium diphosphates $Tl_2Me(H_2P_2O_7)_2 \cdot 2H_2O$, Me = Mg, Mn, Co, Ni and Zn. Synthesis, single crystal X-ray structures and powder X-ray structure of the Mg phase. *Z. Kristallogr.* **2008**, *223*, 448–455. [CrossRef]

36. Capitelli, F.; Harcharras, M.; Assaaoudi, H.; Ennaciri, A.; Moliterni, A.G.G.; Bertolasi, V. Crystal structure of new hexahydrate dicobalt pyrophosphate $Co_2P_2O_7 \cdot 6H_2O$: Comparison with $Co_2P_2O_7 \cdot 2H_2O$, α-, β- and γ- $Co_2P_2O_7$. *Z. Kristallogr.* **2003**, *218*, 345–350. [CrossRef]

37. Capitelli, F.; Khaoulaf, R.; Harcharras, M.; Ennaciri, A.; Habyby, S.H.; Valentini, V.; Mattei, G.; Bertolasi, V. Crystal structure and vibrational spectroscopy of the new acidic diphosphate $(NH_4)_2Zn(H_2P_2O_7)_2 \cdot 2H_2O$. *Z. Kristallogr.* **2005**, *220*, 25–30. [CrossRef]

38. Shannon, R.D. Revised effective ionic radii and systematic studies of interatomic distances in halides and chalcogenides. *Acta Crystallogr. A* **1976**, *32*, 751. [CrossRef]

39. Carnall, W.T.; Fields, P.R.; Rajnak, K. Electronic energy levels in the trivalent lanthanide aquo ions. I. Pr^{3+}, Nd^{3+}, Pm^{3+}, Sm^{3+}, Dy^{3+}, Ho^{3+}, Er^{3+}, and Tm^{3+}. *J. Chem. Phys.* **1968**, *49*, 4424–4442. [CrossRef]

40. Cao, C.; Yang, H.K.; Chung, J.W.; Moon, B.K.; Choi, B.C.; Jeong, J.H.; Kim, K.H. Hydrothermal synthesis and white luminescence of Dy^{3+}-doped $NaYF_4$ microcrystals. *J. Am. Ceram. Soc.* **2011**, *94*, 3405–3411. [CrossRef]

41. Sun, J.; Cui, D. Synthesis, structure, and thermally stable luminescence of Dy^{3+}-doped $Na_3YSi_2O_7$ host compound. *J. Am. Ceram. Soc.* **2014**, *97*, 843–847. [CrossRef]

42. Cavalli, E.; Bettinelli, M.; Belletti, A.; Speghini, A. Optical spectra of yttrium phosphate and yttrium vanadate single crystlas activated with Dy^{3+}. *J. All. Compd.* **2002**, *341*, 107–110. [CrossRef]

43. Jayasimhadri, M.; Ratnam, B.V.; Jang, K.; Lee, H.S.; Chen, B.; Yi, S.-S.; Jeong, J.-H.; Moorth, L.R. Greenish-yellow emission from Dy^{3+}-doped Y_2O_3 nanophosphors. *J. Am. Ceram. Soc.* **2010**, *93*, 494–499. [CrossRef]

44. Carnall, W.T.; Crosswhite, H.; Crosswhite, H.M. *Energy Level Structure and Transition Probabilities in the Spectra of the Trivalent Lanthanides in LaF_3*; Argonne National Lab: Argonne, IL, USA, 1978.

45. Blasse, G.; Dirksen, G.J. Luminescence of Eu(III) in $(NH_4)_3YCl_6$: Nonradiative transitions induced by the second coordination sphere. *J. Sol. State Chem.* **1992**, *96*, 258–262. [CrossRef]

46. Blasse, G.; Brixner, L.H.; Mroczkowski, S. The electronic and vibronic transitions in the emission spectrum of Gd^{3+} in the yttrium hydroxide structure. *J. Sol. State Chem.* **1989**, *82*, 303–306. [CrossRef]

47. Sytsma, J.; van Schaik, W.; Blasse, B. Vibronic transitions in the emission spectra of Gd^{3+} in several rare-earth compounds. *J. Phys. Chem. Solids* **1991**, *52*, 419–429. [CrossRef]

48. Brixner, L.H.; Crawford, M.K.; Blasse, G. Optical luminescence of electronic and vibronic transitions in $Gd_{2-x}Y_x(SO_4)_3 \cdot 8H_2O$. *J. Sol. State Chem.* **1990**, *85*, 1–7. [CrossRef]

49. Nash, K.L.; Dennis, R.C.; Gruber, J.B.; Sardar, D.K. Intensity analysis and energy-level modelling of Nd^{3+} in $Nd^{3+}:Y_2O_3$ nanocrystals in polymeric hosts. *J. Appl. Phys.* **2009**, *105*, 033102. [CrossRef]

50. Kindrat, I.I.; Padlyak, B.V.; Lisiecki, R.; Adamiv, V.T. Spectroscopic and luminescent properties of the lithium tetraborate glass co-doped with Nd and Ag. *J. Alloys Compd.* **2021**, *853*, 157321. [CrossRef]

51. Moorthy, L.R.; Rao, T.S.; Jayasimhadri, M.; Radhapathy, A.; Murthy, D.V.R. Spectroscopic investigations of Nd^{3+}-doped alkali chloroborophosphate glasses. *Spectrochim. Acta A Mol. Biomol. Spectrosc.* **2004**, *60*, 2449–2458. [CrossRef]